ANALYSIS OF MGS TES DATA OVER ACIDALIA PLANITIA AND CYDONIA MENSAE: COMPOSITIONAL EVIDENCE FOR HYDROVOLCANIC ACTIVITY? W.H. Farrand[1] and L.R. Gaddis[2], [1]Space Science Institute, 3100 Marine St, Suite A353, Boulder, CO 80303, farrand@colorado.edu, [2]U.S. Geological Survey, Flagstaff, AZ.

Introduction: The very dark terrain of Acidalia Planitia, Mars, has been recognized as unique on the basis of its relatively low elevation, its role as a receptical for water released from major outflow channels such as Kasei and Ares Valles, and, recently, on the basis of compositional distinctiveness [1,2]. If a northern ocean existed [3], much of Acidalia Planitia would have been submerged below its waters. Large portions of Acidalia Planitia have been described as being volcanic in origin [4]. Given the confluence of volcanic activity and the likely presence of water (from a standing ocean, ice sheets, or just transient flows of water), it is reasonable to look for signs of water/magma interactions in Acidalia. Indeed, a number of previous workers have suggested that some landforms in Acidalia are equivalent to terrestrial tuyas and moberg hills [5], while others might be rootless cones and/or tuff cones [6-8].

For this study, Mars Global Surveyor (MGS) Thermal Emission Spectrometer (TES) emissivity data for Acidalia Planitia and Cydonia Mensae (**Figure 1**) were assembled and used to examine the surface mineralogy of these areas. Analyzing TES data for high latitude locales such as Acidalia presents a challenge since the surface temperatures over these regions is inherently lower than for equatorial locales. In this report, analyses of TES data are described and results are evaluated for potential compositional evidence for hydrovolcanic activity in Acidalia and Cydonia.

TES data. TES emissivity and albedo data were extracted using the ISIS program "vanna" (an interface to the ASU "vanilla" software) over a region from 5 to 35° west longitude and 24 to 44° north latitude. These nadir TES data have surface temperatures between 250° to 350° K, incidence angles between 0 and 80°, and emission angles less than 10°. To reduce noise in the TES data, individual detector elements were averaged for each orbit and instrument observation sequence (i.e., ock and ick), and average emissivity values were reported for each detector footprint. Thus each pixel in the dataset represents a single TES detector, but may be averaged with as many as six other pixels. This intermediate dataset was sorted so that "hotter" pixels were on the bottom of the list. The ISIS "lev2raster" routine was used to overlay the pixels with the warmer data on top, replacing overlapping/underlying cooler pixels. The TES lambert albedo image (**Figure 2**) shows the lower elevation, very dark terrain of Acidalia Planitia and the brighter, higher elevation Cydonia Mensae at the lower right. The brightness of a derived dust index image (after [9]; **Figure 3**) shows an almost inverse correlation with albedo; however, lower values in the dust index image indicates more dust cover thus Cydonia has more dust than does Acidalia.

Analysis and Results. The TES data were analyzed using a minimum noise fraction (MNF) transform ([10]; a variant of the Principal Components transformation) and an implementation of the linear deconvolution algorithm described in [11] and in common use for compositional analyses with TES data [eg., 12]. A three-band composite of the MNF transformed data is shown in **Figure 4**. The ordered MNF transform results can be interpreted as indices of image quality; lower band numbers have less noise and higher bands have more. The Cydonia Mensae highland terrain southeast of Acidalia is red in Fig. 2 (bright in MNF band 1). Green regions are bright in MNF band 4, and blue regions are bright in MNF band 20. The distribution of green units in Acidalia highlights the north/south compositional dichotomy that has been noted by others [13, 14]. The blue unit shows major impact craters in this region. The presence of coherent spatial units in the MNF bands is indicative of surface units of distinct composition and suggestive of diagnostic mineralogic information in the emissivity spectra.

The spectral unmixing or linear deconvolution of TES data was perfomed with a library of 39 spectra including 6 atmospheric spectra and a blackbody (Table 1). After calculation of mineral fractions from each endmember in the library, the fractions of atmospheric components were subtracted from the data to produce an "atmosphere-removed" or surface emissivity dataset [15].

Trends in the derived mineral fraction images include: The Cydonia Mensae bright region had high fractions on the order of 20 to 30% of Pahala Ash and also relatively high fractions (above 15%) of fine-grained, red hematite. Although under the 10% detection limit [16], higher fractions of anhydrite and gray hematite in Acidalia than in Cydonia were noted. Acidalia also had higher fractions of basaltic glass than were noted in an analysis of a similarly derived dataset of Syrtis Major. High basaltic glass fractions in Acidalia have been previously observed [12]. Higher

fractions of the Na/K glass endmember than are present in Syrtis Major were noted as were spatial patterns that are under review. Observed fractional abundances are also being compared to TES-derived thermal inertia and surface dust index as well as to gridded MOLA topography.

Conclusions. Results obtained from the TES data are consistent with, but do not require, aqueous alteration and/or hydrovolcanic activity. The noted high fractions of basaltic glass are especially tantalizing given that water/magma interactions produce copious amounts of basaltic ash [17]. Work is ongoing to link compositional signatures to landforms observed in MOC data that resemble hydrovolcanic edifices [18]. To conclusively link spectroscopic signatures to surface features may require the spatial and spectral resolution of the planned CRISM instrument [19]. The ability to map different types of hydrovolcanic tephras in hyperspectral data has been demonstrated on terrestrial sites by [20].

Table 1. Library spectra used in linear deconvolution.

Dust low CO_2 [12]	Dust high CO_2 [12]
H_2O ice cloud (hi-lat) [12]	H_2O ice cloud (lo-lat) [12]
CO_2 gas [12]	H_2O gas [12]
Quartz 055 [21]	Andesine 001 [21]
Albite 026 [21]	Microcline 043 [21]
Labradorite 063 [21]	Bytownite 177 [21]
Anorthite 178 [21]	Augite 071 [21]
Augite 147 [21]	Diopside 161 [21]
Actinolite 028 [21]	Bronzite 026 [21]
Enstatite 030 [21]	Hedenbergite 215 [21]
Hornblende 173 [21]	Fayalite 167 [21]
Forsterite 008 [21]	Chlorite 040 [21]
Muscovite 020 [21]	Kaolinite 186 [21]
NaMontmorillonite201[21]	Gray Hematite 050 [21]
Gypsum 078 [21]	Anhydrite 081 [21]
Calcite 098 [21]	Dolomite 111 [21]
Pahala Ash [22]	Na/K glass [23]
Silica glass [23]	Goethite [24]
Nanophase hematite [24]	Red hematite [24]
PB90-4 Basaltic glass [25]	

Acknowledgements. This work is being funded by NASA Office of Space Science Mars Data Analysis Program grant NAG5-10577. We would like to thank J. Bandfield, J. Johnson, V. Hamilton and M. Lane for providing spectra used in the linear deconvolution analysis.

References. [1] Bandfield et al. (2000) *Science 287*, 1626. [2] Wyatt and McSween (2002) LPS XXXIII #1702. [3] Head J. et al. (1999) *Science*, *286*, 2134. [4] Scott and Tanaka (1986) USGS map I-1802a. [5] Allen (1979) *JGR*, *84*, 8048. [6] Hodges and Moore (1994) USGS Prof. Paper 1534. [7] Frey et al. (1979) *JGR*, *84*, 8075. [8] McGill, (2002) *LPS XXXIII* #1126. [9] Ruff and Christensen (2001) 1st MER Landing Site Workshop, #9026. [10] Green et al. *TGARS*, *26*, 65. [11] Ramsey and Christensen (1998) *JGR*, *103*, 577. [12] Bandfield *JGR*, *107*, 9-1. [13] Farrand et al. (2001) *DPS 32*, #62.06. [14] Noe Dobrea and Bell (2002) *LPS XXXIII*, #1931. [15] Smith et al. (2000) *JGR*, *105*, 9589. [16] Christensen et al. (2001) *JGR 106*, 23,823. [17] Sheridan and Wohletz (1983) *J. of Volc. Geotherm. Res.*, *17*, 1. [18] Farrand et al. (2001) *LPS XXXII* #1664. [19] Murchie et al. (2002) *LPS XXXIII* #1697. [20] Farrand, *LPS XXXIV* submitted. [21] Christensen et al. (2000) *JGR, 105*, 9735. [22] Johnson (2002) *JGR, 107*, 10.1029. [23] Hamilton et al. (2001) *JGR, 106*, 14,733. [24] Lane et al. (1999) 5th Mars Conf. #6085. [25] Farrand and Lane (2002) *LPS XXXIII* #1804.

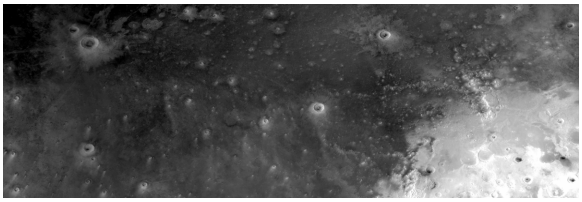

Figure 1. MOC WA mosaic of Acidalia/Cydonia.

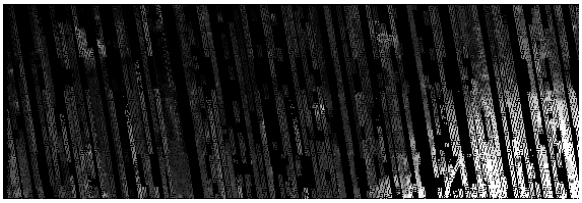

Figure 2. TES albedo of Acidalia/Cydonia.

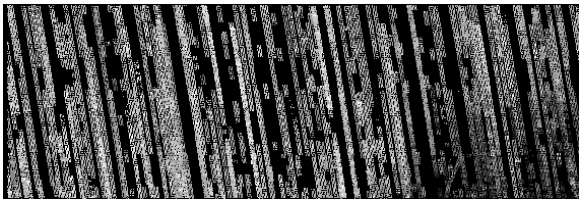

Figure 3. Surface dust index image of Acidalia/Cydonia. Darker regions have greater dust cover.

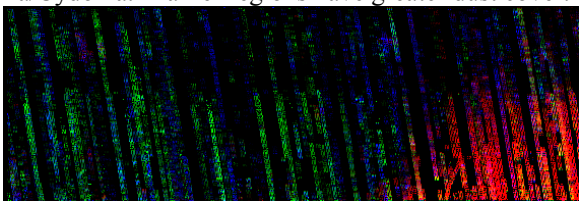

Figure 4. Composite of MNF bands 1 (red), 4 (green) and 20 (blue). MNF 1 highlights the Cydonia bright region, 4 shows the north/south Acidalia dichotomy, and 20 highlights large craters.